Energy Conversion and Management 150 (2017) 890–903

Contents lists available at ScienceDirect

Energy Conversion and Management

journal homepage: www.elsevier.com/locate/enconman

Simulation, implementation and monitoring of heat pump load shifting using a predictive controller

John Allison [a], Andrew Cowie [a], Stuart Galloway [b], Jon Hand [a], Nicolas J. Kelly [a,*], Bruce Stephen [b]

[a] Energy Systems Research Unit (ESRU), Department of Mechanical & Aerospace Engineering, University of Strathclyde, Glasgow G1 1XJ, UK
[b] Department of Electronic & Electrical Engineering, University of Strathclyde, Glasgow G1 1XW, UK

ARTICLE INFO

Article history:
Available online 9 May 2017

Keywords:
Heat pump
Load shifting
Field trial
Building simulation
Predictive control

ABSTRACT

A predictive load shifting controller has been developed and deployed in a low-carbon house near Glasgow, UK. The house features an under floor heating system, fed by an air-source heat pump. Based on forecast air temperatures and solar radiation levels, the controller firstly predicts the following day's heating requirements to achieve thermal comfort; secondly, it runs the heat pump during off peak periods to deliver the required heat by pre-charging the under floor heating. Prior to its installation in the building, the controller's operating characteristics were identified using a calibrated building simulation model. The performance of the controller in the house was monitored over four weeks in 2015. The monitored data indicated that the actual thermal performance of the predictive controller was better than that projected using simulation, with better levels of thermal comfort achieved. Indoor air temperatures were between 18 °C and 23 °C for around 87% of the time between 07:00 and 22:00. However, the performance of the heat pump under load shift control was extremely poor, with the heat being delivered primarily by the unit's auxiliary immersion coil. The paper concludes with a refined version of the controller, that should improve the day-ahead energy predictions and offer greater flexibility in heat pump operation for future field trials.

1. Introduction

The domestic sector faces a range of challenges as the UK attempts to drastically cut its carbon emissions by 2050. Key issues are reducing the overall demand for heat and decarbonising the residual heat loads, which encompass both space heating and hot water provision. If the supply of electricity in the UK is progressively decarbonised at the macro and micro-scales, through the deployment of renewable generation, then the electrification of heat using heat pumps would be an effective means to provide the low-carbon space heating, hot water and possibly cooling required by the domestic sector. However, the widespread adoption of heat pumps would significantly increase power flows on the electricity network. Wilson et al. [1] indicated that a shift of only 30% of domestic heating to heat pumps could result in an increase of 25% in the total UK electrical demand. To mitigate the potential negative impacts of heat pumps, particularly increased peak demand and to reduce or delay network upgrade costs, time-shifting of heat pump demand could become essential.

There have been many papers published, focusing on load shifting of household heat demands and their impacts. For example, Callaway [2] used modelling and simulation to assess the potential for manipulation of large populations of thermostatically controlled loads to follow variable renewable generation. In another modelling-based study, Parkinson et al. [3] designed a controller for distributed heat pump management that also accounted for indoor comfort constraints that often occur when load shifting. Wang et al. [4] modelled the potential for load shedding in a large population of many thousands of unbuffered domestic heat pumps by manipulating of the space heating set point. Patteeuw [5] et al. looked at the potential of load shifting in large populations of buffered domestic heat pumps to reduce carbon emissions from the power system as a whole, with their modelling study, which used linear programming and simple thermal models, showing reductions in power system CO_2 emissions of 1–7% if price based load shifting was implemented.

This paper is primarily concerned with the practicality of, and thermal impact of heat pump load shifting at the level of the individual dwelling. Again, there are many published papers in the

* Corresponding author.
E-mail addresses: j.allison@strath.ac.uk (J. Allison), andrew.cowie@strath.ac.uk (A. Cowie), stuart.galloway@strath.ac.uk (S. Galloway), jon@esru.strath.ac.uk (J. Hand), nick@esru.strath.ac.uk (N.J. Kelly), bruce.stephen@strath.ac.uk (B. Stephen).

http://dx.doi.org/10.1016/j.enconman.2017.04.093
0196-8904/

Nomenclature

ΔT	hysteresis relay temperature (°C)
$\hat{C}$	estimated amount of charge (kW h)
$\overline{\Phi}_{sol}$	daily average solar insolation (W/m^2)
$\overline{T}_{ext}$	daily average external air temperature (°C)
σ_f	signal standard deviation
σ_m	characteristic length scale
Φ_H	heat output (W)
Φ_{on}	hysteresis controller on heat flux (W)
C	amount of charge (kW h)
C^*	enhanced estimated amount of charge (kW h)
d	number of variables in Gaussian process training set
$k(\boldsymbol{x}_i, \boldsymbol{x}_j)$	Gaussian process covariance function
$m(\boldsymbol{x})$	Gaussian process mean function
P	heat pump power (kW)
P_{max}	maximum heat pump power (kW)
R^2	coefficient of determination (1)
$T_{H,set}$	heating set-point temperature (°C)
t_c	duration of charge (h)
T_{db}	dry-bulb air temperature (°C)
T_{err}	control error temperature (°C)
T_{max}	maximum temperature (°C)
T_{mean}	mean temperature (°C)
T_{min}	minimum temperature (°C)
T_{mrt}	mean radiant temperature (°C)
T_{off}	hysteresis controller off temperature (°C)
T_{on}	hysteresis controller on temperature (°C)
T_{op}	operative temperature (°C)
t_{sim}	start time for simulated flexible load-shift (h)
T_{sp}	radiative set-point temperature (°C)
U-value	steady-state thermal transmittance (W/(m^2 K))

literature looking at this area. For example, Hong et al. [6,7] found that shifts in heat pump operating times of up to 6 h were possible in thermally improved dwellings, but only with the addition of up to 500 l of hot water thermal buffering. Arteconi et al. [8] investigated the use of buffering in less well-insulated buildings, indicating that up to 800 l of buffering would be required to deliver only 1 h of load shifting. Kelly et al. [9] investigated load shifting of heat pump demand to off-peak periods in low carbon housing and found that to avoid discomfort up to 1000 l of hot water thermal buffering would be required. Renaldi et al. [10] used cost optimisation to identify optimum storage sizes for load shifting heat pump operation to off peak. Their modelling used synthetic heat loads and a system that featured back up immersion heating. The resulting cost-optimised store sizes (200–300 l) were considerably smaller than those identified using engineering modelling approaches [6–8,9,10].

In all of the papers cited, the authors used modelling to assess the potential for load shifting with a variety of technologies and in different operating contexts. Whilst this provides useful data for technology development and future network planning, modelling has its limitations in that it cannot highlight practical problems associated with the application and implementation of domestic heat load shifting, such as poorly functioning equipment or failure to achieve predicted levels of thermal comfort. A range of studies have indicated that the thermal modelling of buildings and their systems tend to provide over optimistic results compared to what is achieved in reality (e.g. Norford et al. [11], Knight et al. [12]), particularly in relation to energy use. Ryan and Sandqusit [13], recommend that to improve accuracy models are calibrated against empirical data to improve performance. In this paper the performance of a load shifting system was modelled, with the results used as the basis for the design of a day-ahead, predictive load shifting controller. Importantly, the model used was calibrated using monitored data and the energy and thermal performance of the controller operating in a real building was then monitored and assessed.

1.1. Novelty of the work

The novel features of the work reported are (1) the use of a calibrated simulation model to identify the parameters for the a load shift controller, which was then implemented in a real building; (2) monitoring of the performance of the controller and heating equipment over several weeks; and (3) the performance was assessed from the perspective of both energy use and the resulting indoor thermal conditions – so the comfort conditions achieved in the test building under the load shifting control are a key metric for the success or failure of the load shifting approach.

2. Methodology

The work described in this paper involved six distinct stages of activity. These were as follows.

1. Deployment of monitoring equipment and acquisition of performance data;
2. development and calibration of a simulation model of the test house;
3. use of the model to identify the parameters for a predictive control algorithm;
4. assessing the virtual effectiveness of load shifting using simulation;
5. implementation of the load shift controller in the real test house; and
6. monitoring and assessment of actual performance under load shifting.

The results emerging from the monitoring of the load shifting controller and systems performance highlighted important issues regarding heat pump operation under intermittent load shifting control and also allowed the load shift control algorithm to be further refined.

2.1. Details of the test house

The building used for the tests the Applegreen House is located at BRE Ltd's Innovation Park, Motherwell near Glasgow (55.78°N, 3.99°W). The house is intended to be a demonstration of a mass-market, low-cost, modular-build, low-carbon house. The building is shown in Fig. 1. The house is steel framed, has a slab-on-grade concrete foundation with a flat-roof construction. The roof is weatherproofed using bituminous felt. The building is clad in insulated panels, which are externally rendered; the upper half of the building also features external timber cladding.

Windows are double-glazed. The interior of the house is finished with plaster-on-stud and carpeted throughout.

The house has a total floor area of 127 m^2 spread over an upper and lower floor and has an internal volume of 304 m^3. As the house is a test facility, it was unoccupied during the reported experiments; the implications of this are discussed later in the paper.

Heating and hot water are provided by a 3/5 kW NIBE F470 air source heat pump – the heat delivered to the house is recovered

Fig. 1. The Applegreen house at BRE Innovation Park, Motherwell.

from the exhaust air. The maximum heat pump output is 3 kW; a 5 kW direct electric immersion coil is also available if required.

The heat pump was coupled to a mechanical ventilation system with the evaporator located in the extract duct. The heat pump evaporator therefore acted as a heat recovery device. The mechanical ventilation system delivered 55 l/s of outside air or approximately 0.65 AC/h. Unlike the tank-buffered heat pump systems, which feature in the literature (e.g. [7,9]), the heat pump serves an underfloor heating system, which supplies the lower and upper floors. The heat is delivered into pipes embedded in the floor screed, which is approximately 70 mm deep. The heavyweight floor screed therefore acts as the heat store and thermal buffer between the heat pump and the interior of the house.

The heat pump includes an internal 170 l hot water tank. A system schematic is shown in Fig. 2. However, hot water demand was not considered in these tests.

The house also features a 3 kW PV array on the rooftop which feeds into the house supply after power conditioning and inversion.

2.2. Monitoring and data acquisition

Prior to the development of the simulation model and field trial of the predictive controller, the house was instrumented with the variation in indoor temperatures and external climate data monitored for several weeks in July and August 2015.

The data acquisition system used a wireless Eltek RX250AL Receiver/Logger along with three Eltek wireless transmitters; two of these were used to measure indoor temperature and relative humidity, and the final transmitter was used to measure the current at the consumer unit. During the monitored period, total electrical amperage was recorded; this was converted into watts, assuming a voltage of 230 V.

A laptop running a customised data acquisition algorithm polled the logger for monitored data and uploaded this via a web service interface to a UK-based cloud server at 10 min intervals. Each upload held two sets of 5 min data readings from the transmitters.

The instrumentation also included a rooftop weather station supplied by Campbell Scientific, which measured direct and diffuse solar radiation, external air temperature and RH, wind speed and direction. Readings were recorded at 5 min intervals. This data was downloaded manually and merged with the data from the logger. An example of the collected data is shown in Fig. 3, which shows the variation in indoor temperatures and external conditions.

The air leakage of the building was checked using a blower door test. The results indicated that the fabric leakage rate was 3 air-changes-per-hour when pressurised to 50 Pa. Under normal operating conditions this translates to leakage rate of 0.06 air-changes-per-hour.

The initial measurements of the heat pump system indicated that almost all of the heat was supplied by the 5 kW immersion coil due to a low return temperature from the under floor heating circuit preventing the compressor from operating. The low temperature was the unavoidable result of the heat pump being run intermittently during off peak tariff periods for the tests described in this paper. The work therefore proceeded on the assumption that

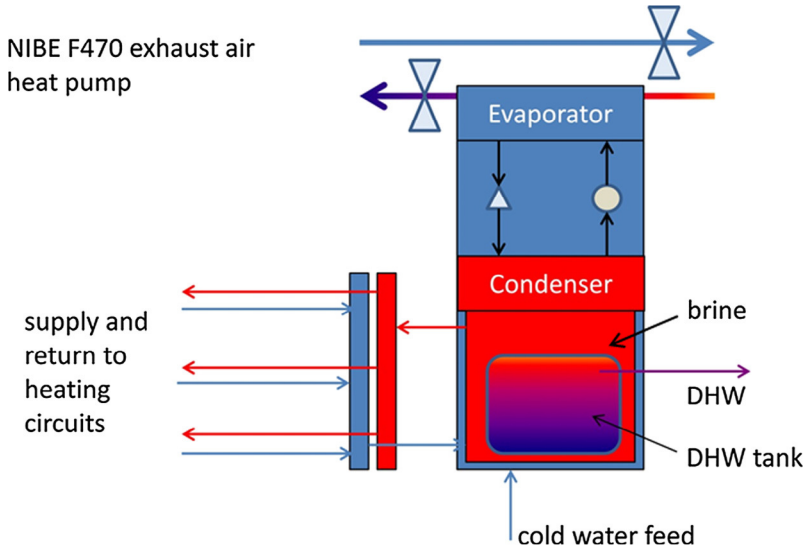

Fig. 2. Schematic of air source heat pump system.

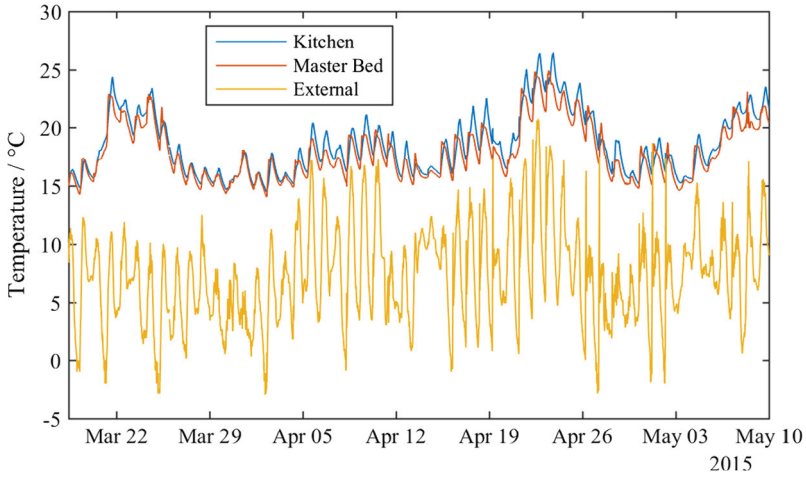

Fig. 3. Example of monitored data.

the heat supplied from the heat pump would be the 5 kW from immersion heater output; this was later confirmed in the analysis of the data from the load shift control tests.

2.3. Simulation model and calibration

A model of the test house was developed for the ESP-r building simulation tool [14]. The wireframe 3-D geometry of the model is shown in Fig. 4a. An ESP-r model is a thermodynamic representation of a building, which typically comprises three core constituents.

- The 3-D geometry of the building is divided into thermal zones, a zone being a notionally enclosed volume within the building, typically corresponding to a specific room. The zone volume is bounded by surrounding surfaces, such as an external wall, internal wall, window, floor, etc. The enclosed space can be modelled at different resolutions: typically the space is modelled as a well-mixed volume at a homogeneous temperature, with heat transfer coefficients used to account for phenomena such as stratification; alternatively the volume can be replaced by a CFD 'domain' [14]. The latter approach has been adopted in this case as this has been demonstrated to provide sufficient accuracy for systems and controls modelling [15]. However, if the function of the analysis was ventilation analysis then the CFD approach would be more appropriate.
- Materials data – each surface has one or more layers that correspond the material layers seen in the real building, with each

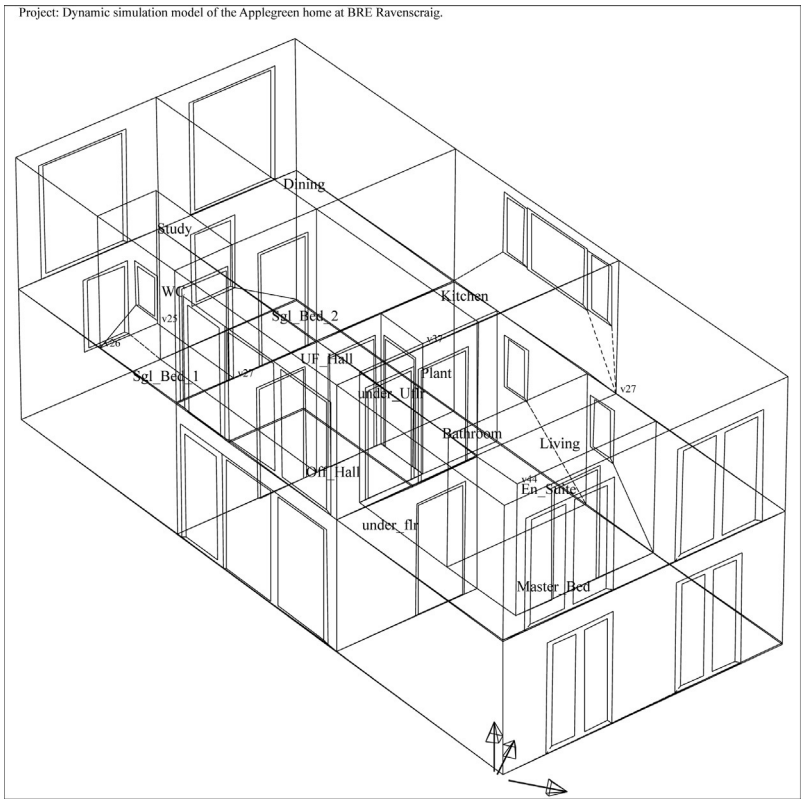

Fig. 4a. The ESP-r geometric representation of the Applegreen house.

layer comprising a specific material type. ESP-r uses a large materials database, which holds information on the following material properties for a wide range of common building materials: conductivity k, density ρ, specific heat c_p, absorptivity and emissivity (–). Additional data is held for transparent materials relating to solar transmission τ, reflection γ and absorption α, at different angles of incidence (0, 40, 55, 70, 90°).

- The geometric and materials data is augmented with schedules that define the magnitude and time variation of internal heat gains from occupants and equipment along with user defined heating control set points, which can be used in the calculation of the time varying heat demand for the building.

The core ESP-r model described above can be used extract various dynamic performance characteristics such as the variability in indoor temperatures, heat fluxes through surfaces, the heating power required to maintain set point temperature in zones, etc.

The resolution of the core model can also be improved with the addition of one or more networks, which are a series of interlinked components. Networks can be used to define the building's HVAC system in detail [14], or to describe bulk airflow paths [16], or the building's renewable energy and electrical systems [17] (where appropriate). In the model described here, an airflow network model was used to determine the bulk buoyancy and pressure driven air flow between zones along with pressure and buoyancy driven infiltration and influence of mechanical ventilation. A schematic of the airflow network is shown in Fig. 4b. At each time step boundary pressures were calculated at external nodes based on wind conditions, and the pressures at internal nodes and airflow through each connection were calculated iteratively.

The house model is available for examination and use, and can be download from: http://fits-lcd.org.uk/file_uploads/Other/173158__Applegreen_Calibrate.tar.gz. ESP-r is available from: https://github.com/ESP-rCommunity/ESP-rSource.

A summary of the geometric and fabric details of the model is provided in Tables 1a and 1b.

The mathematical basis of ESP-r has been described exhaustively elsewhere by Clarke [14], so only a summary is provided here. In the tool, a building model (zones, surfaces, networks) are decomposed into thousands of control volumes, a control volume being an arbitrary region of space to which conservation equations for energy (thermal and electrical), continuity, momentum, species can be applied and one or more characteristic equations formed. The number of equations depends on the resolution of the model. In this case only the energy and continuity equations are required for each control volume. A typical model of a building will contain thousands of such volumes, with sets of equations extracted and grouped according to the physical system (e.g. transfer, fluid flow, power flow, etc.). The equations that describe the heat transfer associated with the building fabric are linearised and solved directly, using a mixed implicit-explicit formulation that is unconditionally stable. The bulk fluid flow and power flow equations (if required) are solved iteratively, and converge for the vast majority of cases. The ESP-r tool and its solution method have been the subject of extensive validation activities over many years, these are described by Strachan et al. [17].

The solution of these equations sets with real time series climate data, coupled with control and occupancy-related boundary conditions yields the dynamic evolution of temperature, energy and fluid flows within the building and its supporting systems.

The model's predictions of indoor air temperature were calibrated using the weather and indoor temperature data collected in the months leading up to the setting-up of the load shifting experiment. This calibration was a multi-stage process that involved iteratively manipulating the characteristics of the air flow network flow connections to the exterior of the building, shown in Fig. 4b, until a match was achieved between average infiltration and the value from the blower door test. Next, the monitored heat input (assumed to be equivalent to the measured background electrical demand) was imposed on the model as a heat gain profile; the air flow network connections between the indoor nodes were modified to achieve temperature difference between the two floors broadly commensurate with the monitored data. Finally, building fabric U-values were degraded to account for thermal bridging and other building defects. The wall U-values emerging from this process are as shown in Table 1b.

The air temperature predictions of the model against measured data are shown in Fig. 5. The model typically produces air temperatures within ±1 °C of measured conditions and the model accurately follows the trends in temperature fluctuations seen in the

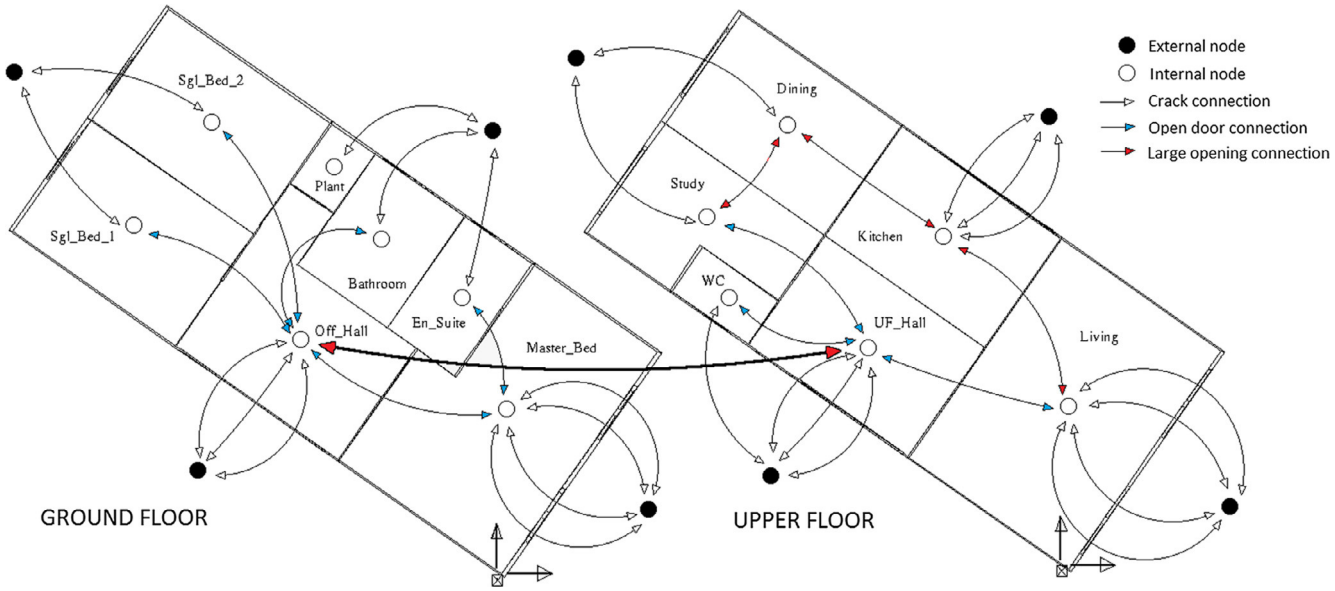

Fig. 4b. Schematic of the airflow network linked with the model.

Table 1a
Summary details of Applegreen house model thermal zones.

Zone name	Level	Volume (m^3)	Glazing (m^2)	Façade (m^2)	Partitions/ceiling/floor (m^2)	Floor (m^2)
Master bedroom	Ground	44.9	3.24	26.4	52.4	18.7
Office & entry	Ground	28.3	9.6	3.6	48.1	11.8
Bedroom 1	Ground	25.4	0.9	15.1	37.1	10.6
Bedroom 2	Ground	25.4	0.9	15.1	37.1	10.6
Plant room	Ground	3.6	0	2.5	12.4	1.5
Bathroom	Ground	13.9	0.3	4.8	29.6	5.8
En-Suite	Ground	10.6	0.3	3.6	25.6	4.4
Living	Upper	50.8	11.2	48.4	27.5	21.2
Upper hall	Upper	25.2	9.5	14.2	29.0	10.5
WC	Upper	5	0.3	6.3	11.8	2.1
Study	Upper	20.5	12.4	17	19.5	8.5
Dining	Upper	25.4	18.9	23.6	10.6	10.6
Kitchen	Upper	25.2	14.9	17.9	19.8	10.5

Table 1b
Summary details of Applegreen house model internal and external constructions.

Description	Thickness (mm)	Number of layers	Mass per (m^2)	U-value (W/m^2 K)	Area in building (m^2)
Ground level Façade wall	235	7	72.3	0.2	67
Upper level Façade wall	242	5	67.6	0.2	58.8
Thick acoustic partition	165	7	47.5	0.306	55.9
Thin non-acoustic partition	90	3	40.9	1.38	14.1
Thin acoustic partition	95	5	35.0	0.53	74.3
Internal door	50	1	29.2	1.8	29.5
Glazing frame	69	2	44.6	1.46	9.9
Façade glazing	26	3	25	1.21	30.2
Roof (flat)	271	6	109	0.18	63.3
Ground level floor	530	4	677	0.18	63.3
Intermediate floor	435	5	352	0.4	59.6

measured data. The accuracy of the sensors is ±0.1 °C. For the purposes of controller development, this level of accuracy was deemed sufficient.

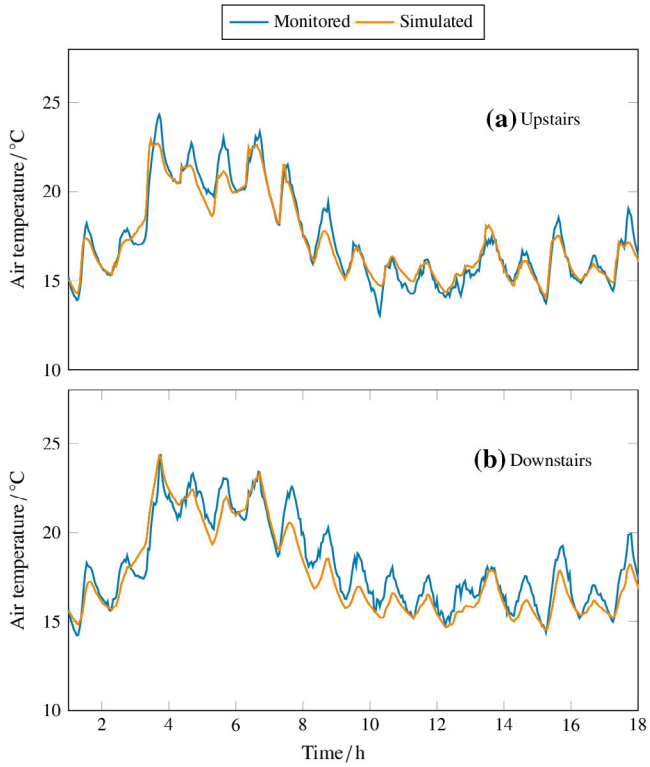

Fig. 5. Monitored and predicted temperatures: (a) Upstairs livingroom; (b) Downstairs kitchen.

It should be noted that because the test house has an under floor heating system, the most accurate measure of thermal comfort would be the dry resultant temperature (DRT), which comprises both the mean radiant temperature and the air temperature. However, the monitoring equipment installed in the test house could only measure the air temperature. The simulation data was analysed to assess the impact of this shortcoming and its potential implications for comfort assessments.

Table 2 shows an analysis of the difference between the air and DRT for the test house with the under floor heating system active. At the minimum house temperature, there was an appreciable difference of over 2 °C between the air and DRT. However, low temperatures such as this tended to occur outside periods of assumed occupancy and the difference at higher temperatures and the overall average difference was less than 1 °C, indicating that for the majority of time, the difference between the two temperatures was small. Based on these findings, it was assumed that the air temperature alone could act as a reasonable proxy for comfort conditions.

2.4. Parameter estimation the load shift control algorithm

The simulation model was used to determine the characteristics of a predictive load shift controller to be installed in the test house. This was a two stage process.

Table 2
Difference between simulated air and dry resultant temperatures.

Gauged temperature	T_{min}/°C	T_{max}/°C	T_{mean}/°C
Zone dry bulb	11.3	35.7	21.2
Mean radiant	15.4	38.4	22.0
Zone dry resultant	13.9	36.0	21.6
Zone dry bulb – resultant	2.6	0.3	0.4

- Using hourly test reference climate data for Glasgow as a boundary condition (19 km from the test house site), the calibrated simulation model was then used to determine the daily heat load (or 'charge'), C (kW h), required to heat the house to 21 °C over an assumed occupied period of (07:00–22:00) as shown in Fig. 6.
- Secondly, a series of simulations were run to determine if the calculated charge could successfully be shifted to off-peak periods whilst still maintaining indoor comfort conditions.

The performance of the house model was simulated over a calendar year at 15 min time intervals. For each simulated time step during the heated period, the model calculated the heat required to maintain temperatures at the set point of 21 °C. This was then aggregated for each day in order to determine the heating charge, *C*, in kW h. The time-varying heat input to the building model is shown at the top of Fig. 7. The area under the graph is the total diurnal charge, *C* that the building required, to reach and maintain comfort conditions. This work relies on the principle that it is possible to alter the shape of the heat load to a 'block' that can then be shifted back into the economy period (see bottom of Fig. 7) by pre-charging the heavy weight floor screed (i.e. thermal storage) using the under floor heating system, which then slowly releases heat into the building during the assumed occupied period (07:00–22:00).

Assuming that the heating system output was fixed at the measured 5 kW, then the duration of charge was calculated from $t_c = C/P$. The load-shifted heating start time (shifting the heating charge into the period 0000–0700 h) was then calculated from Eq. (1).

$$t_s = \begin{cases} 7 - C/P, & C/P \leqslant 7 \\ 24 + (7 - C/P), & C/P > 7 \end{cases} \quad (1)$$

where t_s is the start time (h), *C* is the calculated amount of charge (kW h) and *P* is the heating system capacity (5 kW h).

Note that where the calculated charge and capacity resulted in a charge time of greater than 7 h, the charge would begin prior to midnight (00:00).

The model's estimations of the daily heating charge were used to create a regression algorithm, which could then be implemented in the test house as part of a predictive controller for the heat pump. The predictive controller would estimate the day ahead heating charge based on forecast daily mean temperatures and solar radiation levels.

A linear regression analysis was done on the simulation model output data to generate a polynomial (Eq. (2)) which related the calculated daily heating charge *C* to the corresponding daily average solar radiation $\overline{\Phi}_{sol}$ (W/m^2) and average external temperature $\overline{T}_{ext}$ (°C) – both of which could be derived from the boundary climate data in the model simulations.

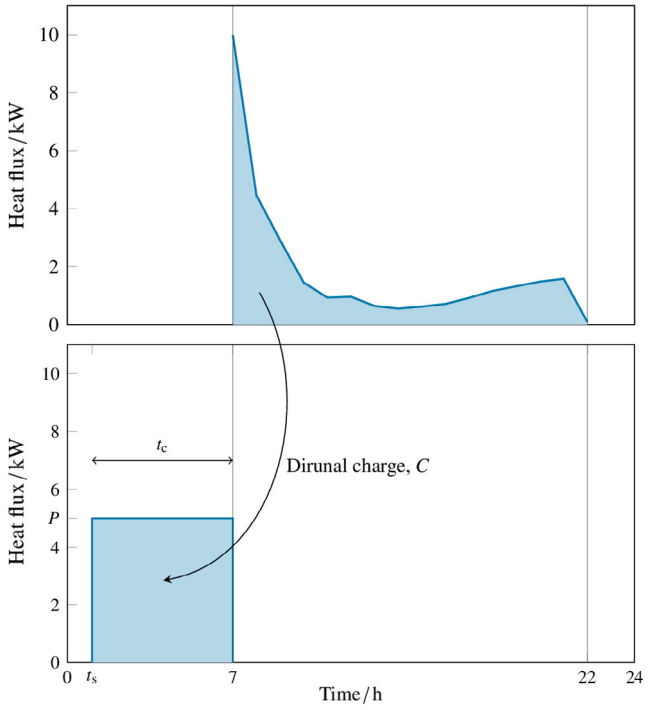

Fig. 7. Visualisation of load-shift controller design with data specific to 2015-03-12. Top figure shows heat flux calculated by basic (ideal) controller. Bottom figure shows the same heat flux re-shaped and shifted to the economy period.

$$\hat{C}(\overline{T}_{ext}, \overline{\Phi}_{sol}) = p_{00} + p_{10}\overline{T}_{ext} + p_{01}\overline{\Phi}_{sol} + p_{20}\overline{T}^2_{ext} + p_{11}\overline{T}_{ext}\overline{\Phi}_{sol} + p_{02}\overline{\Phi}^2_{sol} + p_{21}\overline{T}^2_{ext}\overline{\Phi}_{sol} + p_{12}\overline{T}_{ext}\overline{\Phi}^2_{sol} + p_{03}\overline{\Phi}^3_{sol} \quad (2)$$

where $\hat{C}$ is the estimated heating charge (kW h). The regression coefficients are given in Table 3 with 95% confidence bounds.

The goodness of fit could be analysed via the coefficient of determination, which for the surface defined by (2) is $R^2 = 0.881$, with a corresponding root-mean square deviation of 6.53 kW h, equivalent to a prediction error of $t_{c,RMSE} = 1.3$ h. Note that this measure is scale-dependent, therefore forecasting errors for particular variables will vary.

A refinement of the regression model that improves the regression algorithm's day-ahead charge predictions is undertaken at the end of the paper.

Eq. (2) can be visualised as a control surface as shown in Fig. 8 with the simulated heating charge *C* shown in marked points.

When implemented in the real test house as part of a predictive controller, Eq. (2) would be used to estimate day-ahead heating

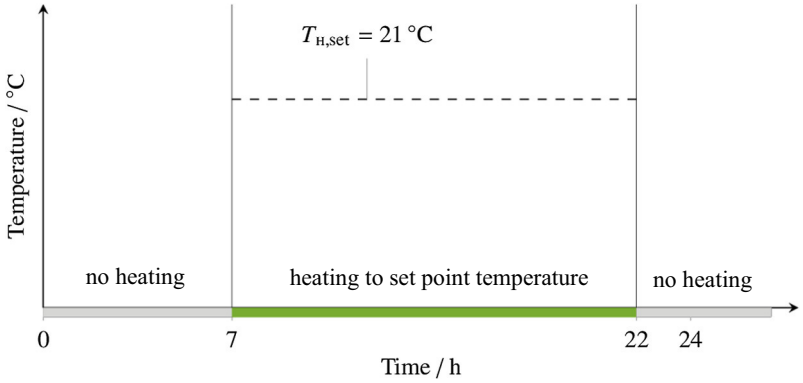

Fig. 6. Control periods used for amount of charge calculations.

Table 3
Coefficients of linear regression model used to predict day-ahead charge with 95% confidence bounds.

p_{00}	73.39 (67.68,79.11)
p_{10}	−1.402 (−2.848,0.04382)
p_{01}	−0.3156 (−0.4126,−0.2187)
p_{20}	−0.1372 (−0.2398,−0.03465)
p_{11}	−0.0105 (−0.02309,0.002098)
p_{02}	0.001044 (0.0004678,0.001619)
p_{21}	0.0008879 (0.00013,0.001646)
p_{12}	9.105×10^{-6} $(-2.84, 4.661) \times 10^{-5}$
p_{03}	-1.477×10^{-6} $(-27.1, -2.45) \times 10^{-7}$

charge $\hat{C}$ (and subsequently start-stop times) based on the day ahead forecast for mean daily temperature and solar radiation.

Note that the equation as shown does not include an allowance for internal occupant gains as the house was not occupied during the tests. However, a similar expression for heating charge, accounting for gains could be developed by including a suitable occupancy pattern in the simulation model.

2.5. Assessing the impact of load shifting using the model

The impact on indoor thermal conditions from shifting the heating charge to off-peak periods (00:00–07:00) was first investigated using the calibrated model, with performance again simulated over a year using the Glasgow climate data set a boundary condition. These simulations used a modified version of the ESP-r tool, which featured the day-ahead heating charge equation (Eq. (2)) integrated into the code; this calculated the next-day heating charge $\hat{C}$ using the following day's temperature and solar data from the model's climate file. The heating charge $\hat{C}$ was delivered into the under floor screed of the model's lower and upper floor constructions, as would happen in the real building.

Assessment of the load shifting controller performance looked at the temperatures achieved in the house between 07:00 and 22:00, specifically assessing if thermal comfort could be maintained after load shift. If temperatures fell below 18 °C or rose above 23 °C, then it was assumed that the occupants would experience discomfort. Fig. 9 shows the amount of time spent inside and outside the comfort range and indicate that the heating charge could be moved to off peak periods without significant discomfort conditions occurring. This was due to two main factors. Firstly, the house fabric was well insulated, which limited temperature drops during unheated periods. Secondly, the upper and lower floor screed (under floor heating) acted as a substantial thermal store – approximately 8.61 m^3 of screed material. Together, the insulated fabric and floor thermal capacity allowed the house to ride through the occupied period of 07:00–22:00 without temperatures dropping significantly. Fig. 10 shows the difference in predicted indoor temperatures between the original simulated control and the simulated load-shifted control.

2.6. Implementation and monitoring of the load shift control in the test house

The load shifting control system implemented in the real test house comprised the following elements.

1. heat pump control interface;
2. monitoring and data acquisition system;
3. load shift controller.

The NIBE heat pump used in the house could be accessed remotely using an internet interface or SMS-based interface. The SMS-based interface was chosen for this work as, unlike the internet interface, the heat pump data could be accessed by 3rd party applications. The SMS interface allowed the heat pump to be switched on and off and also allowed the heat pump internal data to be accessed if required.

Load shift algorithm, based around Eqs. (1) and (2) and supporting software was implemented within a Linux-based cloud server and carried out the following tasks.

- The controller parsed a day-ahead weather forecast from a meteorological web service and used it to calculate the average air temperature and total solar insolation for the following day; this was done at hourly intervals over the preceding day to capture changes in the forecast.
- The control algorithm used the forecast data to calculate the heating charge and associated heating charge time and start/stop times for the heat pump.
- Finally the on/off control signals were passed back to the heat pump in the test house using the Twilio SMS web API which allows cloud based applications to send and receive voice calls and SMS messages.

The communications and data logging system are illustrated in Fig. 11.

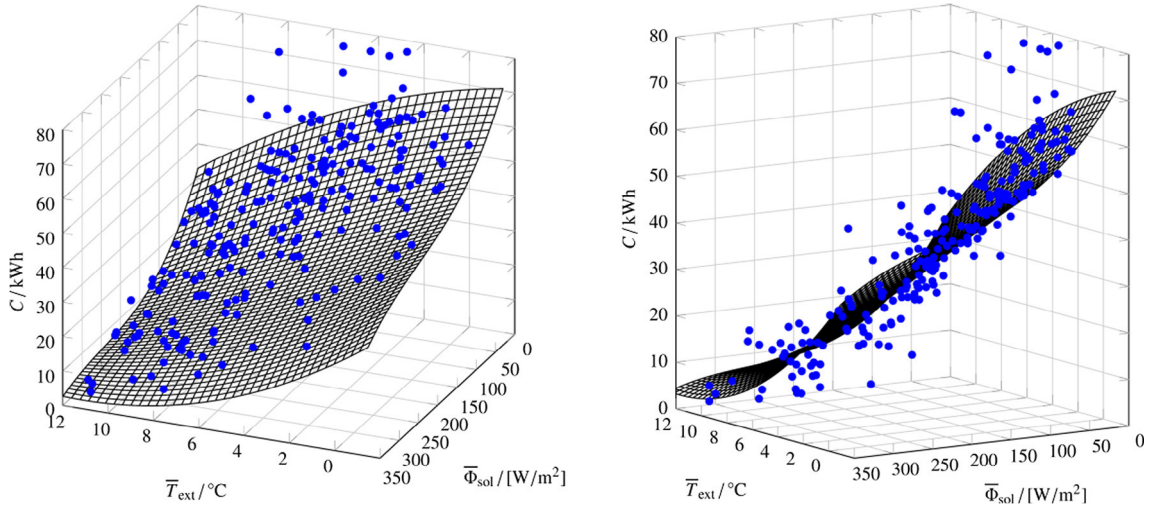

Fig. 8. Plot of surface for $\hat{C}(\overline{T}_{ext}, \overline{\Phi}_{sol})$ with marks for simulated diurnal charge from two perspectives.

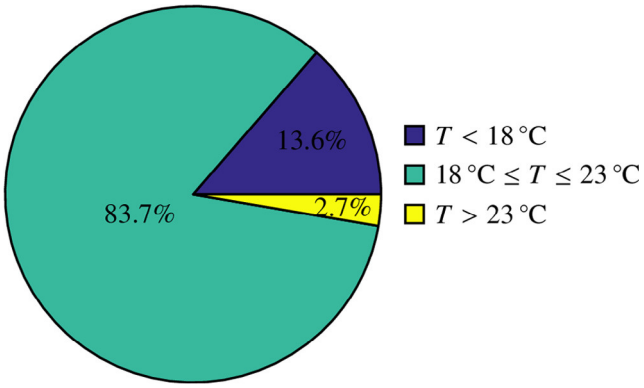

Fig. 9. Time spent in different temperature ranges during the occupied hours under the load-shift controller during days where there was heat input to the house.

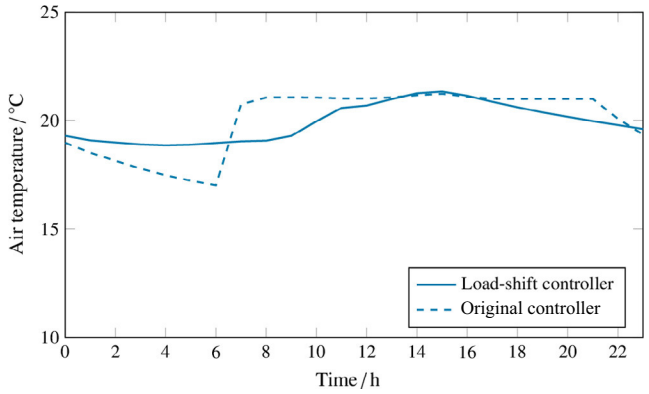

Fig. 10. Dynamic temperature profiles for ideal control and load-shift controller (data shown for 2015-03-12).

The performance of the implemented load shift controller was tested during September 2015, a period when daytime temperatures had dropped enough for the heat pump to run for appreciable periods of time. The field trials comprised two phases.

1. The control system was tested under manual operation: a forecast of the following days weather was obtained and Eqs. (1) and (2) were used to determine the heating start time; this was passed to the heat pump using an SMS message sent from the IF mobile phone application: IF allows tasks to be logic controlled and time scheduled. The purpose of these manual tests was simply to test that the controller, communications to and from the heat pump and the data acquisition system was functioning correctly.
2. Following a successful manual test, the heat pump was then subject to fully automated control using the cloud based controller, this calculated the heating charge and subsequent start/stop times and passed these directly to the heat pump via SMS messages. The output from the controller and monitored data was streamed to a live website.

Note that during the initial testing phase, inspection of the monitored power data indicated that PV generation was being recorded as well as the heat pump power demand. In order to isolate the heat pump energy use, the power produced by the PV had to be removed from the monitored data. To do this, the PV power production was estimated from the monitored climate data using the Araujo-Green method [18] and subtracted from the total recorded wattage.

Once the automated controller was established, the indoor conditions and heat pump power demand were recorded using the monitoring system described previously over a period of approximately three weeks.

3. Results and discussion

Analysis of monitored indoor air temperatures when the fully-automated load shift controller was in operation indicated that they remained between 18 °C and 23 °C for 87% of the time between 07:00 and 22:00, when the heat pump was operated under load shifting control (see Fig. 11). The remaining 13% of the monitored period, temperatures were above 23 °C but less than 25 °C. This performance was actually slightly better than predicted using simulation, which indicated comfort conditions being achieved for approximately 84% of occupied hours.

Fig. 12 shows typical conditions from the test from Sept 8–Sept 12. Higher temperatures occurred when solar gains pushed indoor temperatures above 23 °C. As the heat was pre-delivered into the floor screed, the heating system tested was unable to respond to disturbances after the initial charging period. So, for example, greater than forecast levels of solar radiation would lead to higher indoor air temperatures than predicted. Note that on the two days with the highest solar radiation the calculated charge was zero.

The total energy consumption of the heat pump during the monitored period in September was 434 kW h and the total run time was 91 h. This gave an average power consumption of 4.8 kW and indicates (as was suggested by the initial tests) that the heat supply was almost all from the auxiliary heating coil rather than the heat pump itself. This is evident in the power demand plot in Fig. 12.

3.1. Improving the house model and controller parameter estimation

While the results from the field trial were satisfactory, the work had a number of limitations that could be improved upon. Specifically, these related to further developing the house model used to estimate the controller parameters and improving the load shifting equation and its calibration

1. The model used to calibrate the controller assumed that the temperature in the house was held to 21 °C during occupied periods, whereas a range between 19 and 23 °C would be within comfort limits – avoiding over and under heating. Therefore in the simulation model some hysteresis was added to the representation of heating control, with a 'dead band' added between 19 and 23 °C (Fig. 13). So, when the indoor temperature was or fell below 19 °C the house heating would operate until the temperature reached 23 °C and then remain inoperative until the temperature fell back to 19 °C. This scheme reduces cycling and also increases the potential for flexibility in when the heating system operates (see Fig. 14).
2. Additionally, when estimating the parameters for the controller using Eq. (2), the daily charge C (kW h) was calculated with model, which assumed that the heating flux was delivered directly to the indoor air. In reality, the test house utilised under-floor heating, which would emit a portion of this energy via convection to the air, and via long-wave radiation to the surrounding walls and ceiling; this discrepancy could cause the amount of charge required to be underestimated. Therefore, the calibration model was refined, with the heating input delivered into the floor screed.
3. The regression equation for the day-ahead heating charge used only two parameters: average daily external temperature, $\bar{T}_{ext}$, and average daily solar insolation, $\bar{\Phi}_{sol}$. This doesn't take

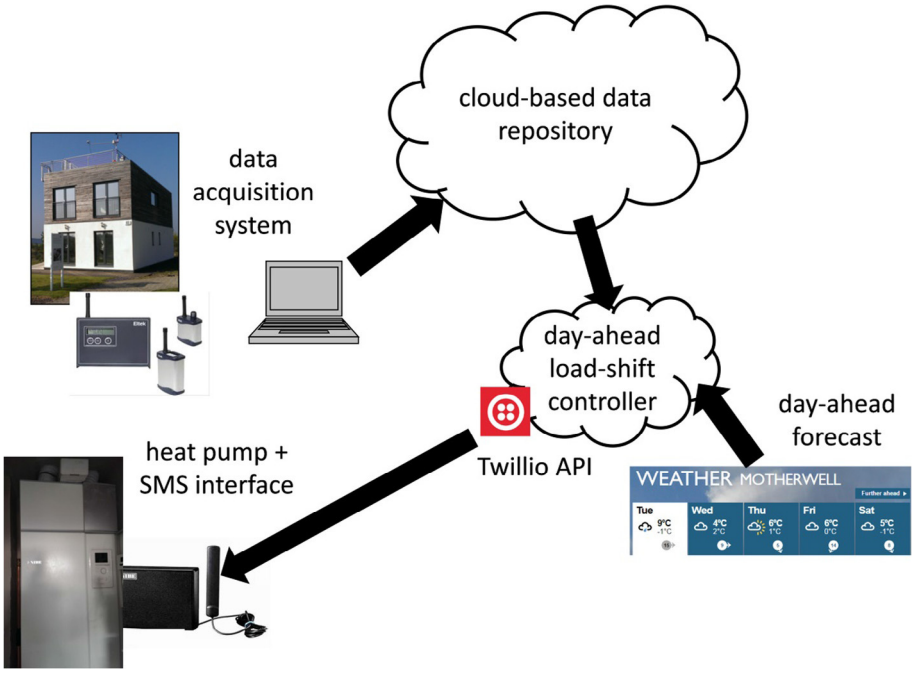

Fig. 11. Illustration of the data acquisition and cloud-based control.

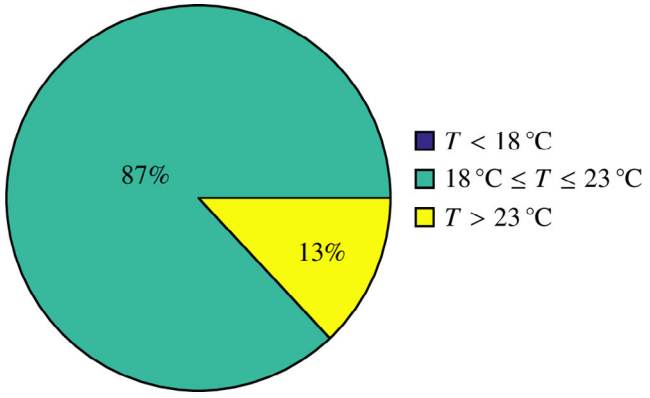

Fig. 12. The breakdown of indoor temperatures over the September test period.

account of the indoor temperature prior to the input from the heat pump. Consequently, a revised version of the controller was developed that accounted for the indoor temperature. Here, instead of the controller parameters being identified using a regression equation, a more sophisticated Gaussian process regression was applied.

The following paragraphs provide more detail on these improvements.

The operation of the heating control was altered to operate with hysteresis, with a switch on point of 19 °C and a switch off point of 23 °C, which would lead to fluctuations of 2 °C above or below the desired zone operative temperature of 21 °C. This can be modelled using a relay shown in Fig. 15, where $\Delta T = 2$ °C, $\Phi_{on} = 10$ kW and $T_{err} = T_{sp} - T_{op}$. T_{op} is the operative temperature of the zone, here

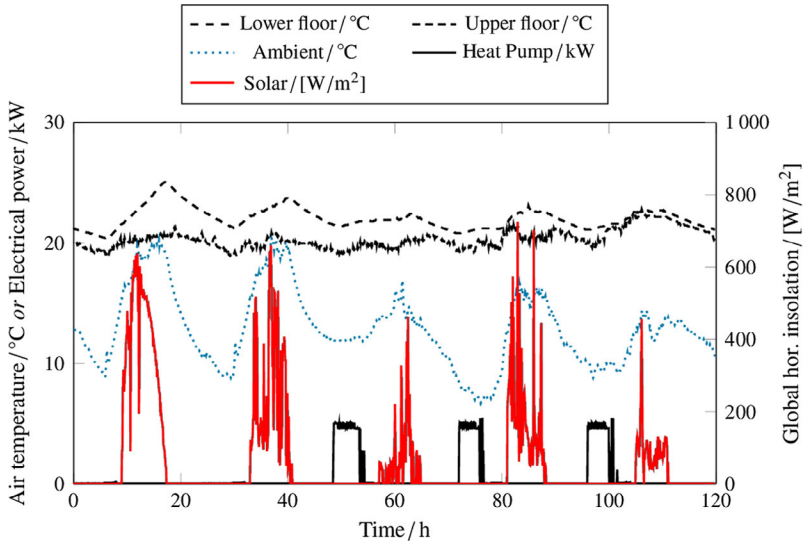

Fig. 13. Measured heat pump charge, external climate, and indoor temperatures for 2015-0908/12.

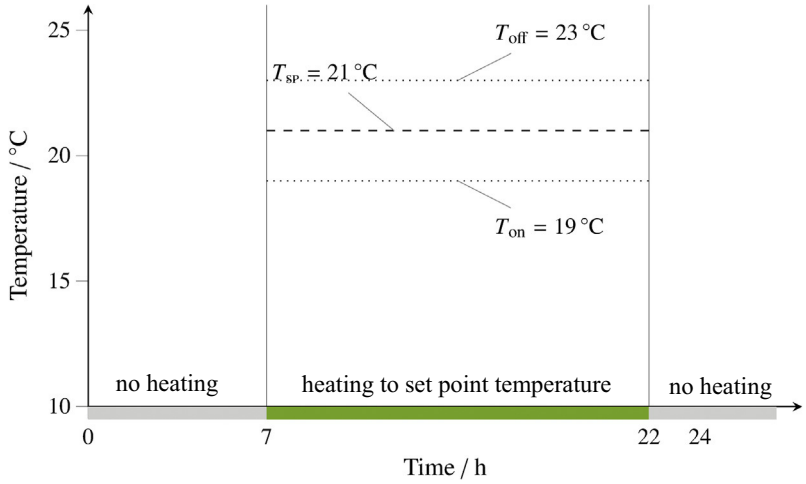

Fig. 14. Ideal mixed-mode control algorithm.

defined as a mix of the zone's dry bulb temperature and mean radiant temperature as

$$T_{op} = (1/2)T_{op} + (1/2)T_{mrt} \tag{3}$$

Operative temperature is a better metric with which to assess comfort than air temperature alone in systems such as under floor heating where a significant component of the heat delivery is radiant.

To reflect this, the heat input to the house model was altered from a purely convective input to a mixed convective/radiant flux:

$$\Phi_{convective} = (2/5)\Phi_H \tag{4}$$

$$\Phi_{radiant} = (3/5)\Phi_H \tag{5}$$

The radiant flux was distributed to the surfaces in the model on an area and emissivity basis, while the convective heat flux was injected to the air in each zone of the model. The total amount of heat flux required during each simulation time step was aggregated per day as $C^* = \int \Phi_H$ in order to determine the new diurnal charge calculation, C^*, in kW h.

To improve parameter estimation for the load shift equation, Gaussian process regression (GPR) was applied. GPR models are nonparametric probabilistic models [19] i.e. the model structure is not predefined as in Eq. (2) but is determined from the available data. This is beneficial as the number of input parameters to the regression increases, the complexity of a predefined polynomial surface would increase rapidly, and selecting a possible candidate function for accurate predictions becomes more difficult. This type of regression model has already been successfully utilised in related fields, such as for short-term wind speed prediction [20], electricity price forecasting [21], and the calibration of building energy models [22].

To construct the GPR model, the algorithm was provided with a training set $\{(\boldsymbol{x}_i, y_i); i = 1, 2, \ldots, n\}$, where $\boldsymbol{x}_i \in \mathbb{R}^d$ and $y_i \in \mathbb{R}$, drawn from an unknown distribution. A GPR model addresses the question of predicting the value of a response variable y_{new}, given the new input vector x_{new}, and the training data.

In this work, the training set was obtained via the annual simulation, with $\boldsymbol{x}_i = (\bar{T}_{ext,i}, \bar{\Phi}_{sol,i}, T_{0,i})$, $d = 3$, $y_i = C_i$, and each $i = 1, \ldots, 365$ represents each i-th day of the year. Compared to the regression model (2), here the GPR model adds the additional parameter T_0, which is the internal air temperature at the beginning of the economy period.

A GPR model is given as

$$f(\boldsymbol{x}) = \mathcal{GP}(m(\boldsymbol{x}), k(\boldsymbol{x}_i, \boldsymbol{x}_j)) \tag{6}$$

where it is fully specified by its mean function $m(\boldsymbol{x})$ and covariance function $k(\boldsymbol{x}_i, \boldsymbol{x}_j)$. It is assumed that it is a zero mean GP with covariance function as the squared exponential kernel function, with a separate length scale for each predictor. It is defined in Eq. (7).

$$k(\boldsymbol{x}_i, \boldsymbol{x}_j|\boldsymbol{\theta}) = \sigma_f \exp\left[-\frac{1}{2}\sum_{m=1}^{d}\frac{(x_{im} - x_{jm})^2}{\sigma_m^2}\right] \tag{7}$$

where for the training dataset obtained via the annual simulation the kernel parameters or hyperparameters are: signal standard deviation is $\sigma_f = 36.092$ and the characteristic length scales are $\sigma_1, \ldots, \sigma_3 = (5.454, 1.6349, 1.7462)$.

The resulting coefficient of determination for the GPR model was $R^2 = 0.954$ (8.3%increase in goodness of fit), with a corresponding root-mean square deviation of 4.62 kW h, equivalent to a prediction error of $t_{c,rmse} = 0.92$ h (29.2% reduction in error). Fig. 16 shows a comparison of predictive results for the multiple linear regression and Gaussian process regression models.

3.2. Further analysis – flexibility in load shifting

The refined house model was employed to assess the potential for flexible load-shifting in the house. Whereby the load-shift was not fixed as in Eq. (1), but could be manipulated to start anywhere within the economy period (00:00–07:00) as long as the day-ahead simulation indicated that the predicted indoor temperatures would be satisfactory. Such flexibility (see Fig. 17) is useful as it can be used to prevent unintended load synchronisation in large-scale, automated load shifting schemes (e.g. [23–25]), which can exacerbate rather than improve the impact of electrified heating on the network.

In the field trial, the calculated charge was always supplied as close as possible to the occupied period i.e. the charge was offset from 07:00. However, the heating charge doesn't always need to be delivered at $7 - C/P$ provided that (1) the calculated length of charge is less than the length of the economy period, and (2) that the indoor environmental conditions will still be satisfactory when the load is shifted to an alternative time window. In this case, there is some flexibility in when the heating charge can be delivered; this provides latitude for improved load manipulation with large numbers of loads. The degree of flexibility is estimated here using a metric giving the number of "flexible hours", t_f, in a diurnal period. This is given by the following equation.

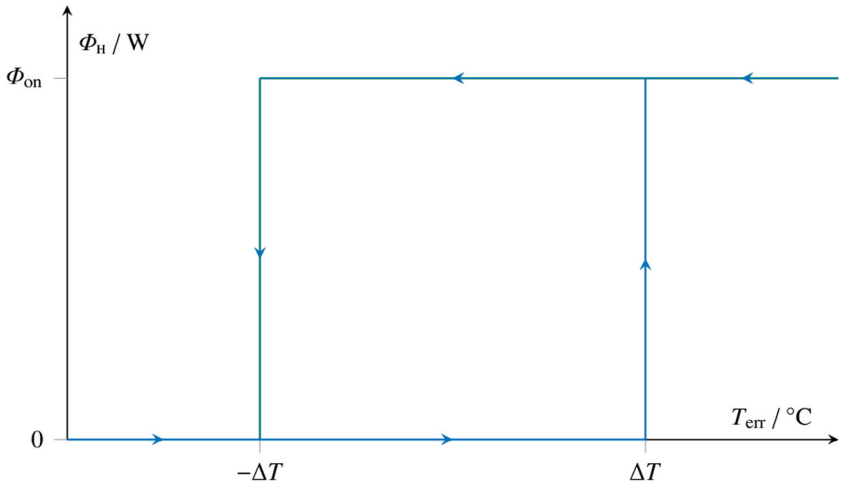

Fig. 15. Hysteresis controller for on/off flux control period.

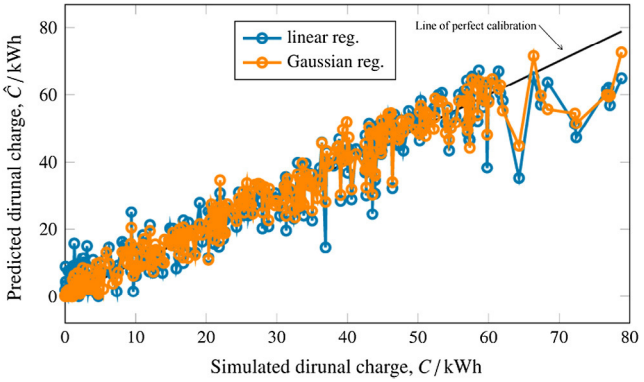

Fig. 16. Comparison of calibration results for the multiple linear regression and Gaussian process regression models.

$$t_f = \begin{cases} 7 - t_c, & t_c \leqslant 7 \\ 0, & t_c > 7 \end{cases} \quad (8)$$

where $t_c = C/P$ is the calculated charge time (h). Note that the amount of flexibility on days with little to zero amount of diurnal charge ($t_c < 20$ min) was not considered as flexible hours, since the actual use of the heat pump was negligible.

The proportion of the flexible hours in (8) that would result in satisfactory indoor environmental conditions was determined via a series of annual simulations whereby the day-ahead diurnal charge was injected at a start time, t_{sim}, of 00:00, 00:30, 01:00 and so on up until 06:30. The new start time for the block of charge is then given by Eq. (9):

$$t_f = \begin{cases} 24 + (7 - t_c), & t_c > 7 \\ 7 - t_c, & (7 - t_{sim}) < t_c \leqslant 7 \\ t_{sim}, & \text{otherwise} \end{cases} \quad (9)$$

The results from each simulation were then compared with the same temperature criteria used in Section 3 in order to find the range of start times that achieved acceptable indoor environmental conditions. Note that the calculated number of hours estimated here will be conservative, as a real occupied building would have additional internal gains from occupants and appliances to contribute to the heat demand.

Fig. 18 shows the number of hours of flexibility in each day of the year and Fig. 19 shows the cumulative number of hours of flexibility for each month of the year.

The modelling analysis indicated that flexibility (the ability to vary when the heat pump operates with and off-peak period) varies seasonally, with the least temporal flexibility being available

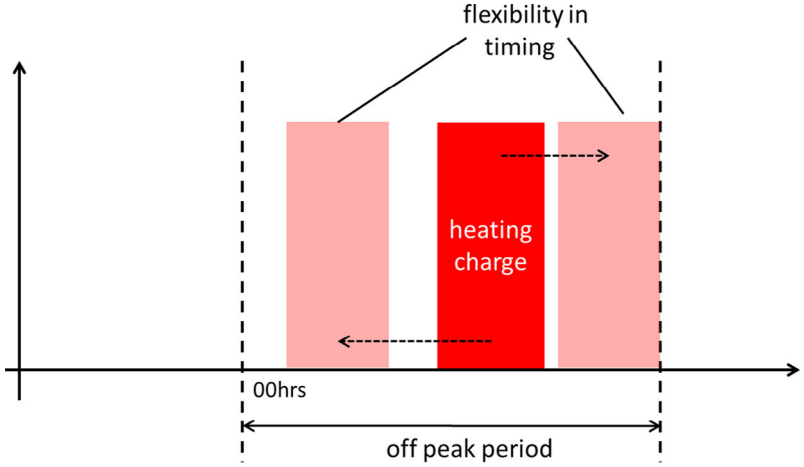

Fig. 17. Illustration of "flexibility" in heat pump operation.

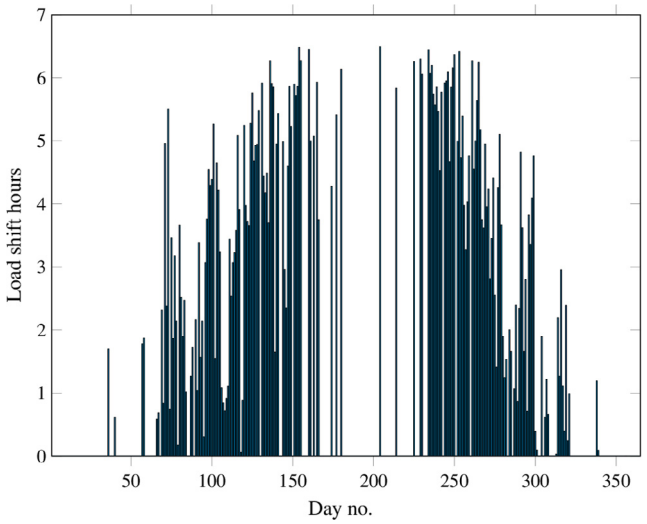

Fig. 18. Daily number of hours of load-shift flexibility.

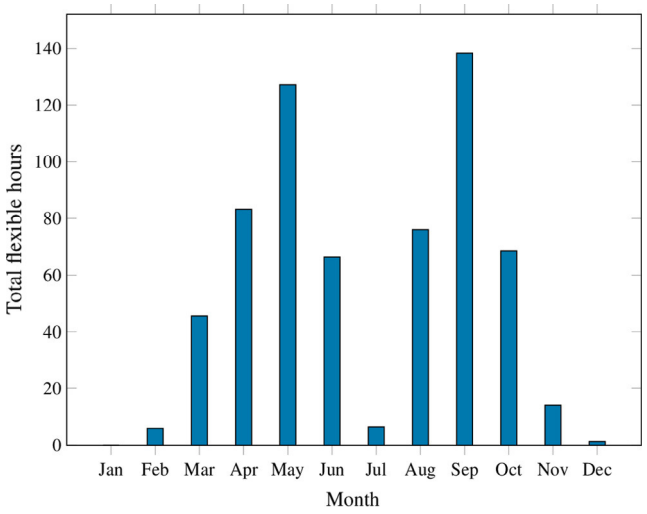

Fig. 19. Monthly cumulative number of hours of load-shift flexibility.

when the load is at its highest such as January and December. This was due to the heating load being such that heat pump needed to be active for all or the majority of off peak hours. Flexibility was also low in July as the heat pump was hardly used.

4. Conclusions

A full scale demonstrator for thermal load shifting in a low carbon house has been established at BRE's Innovation Park near Glasgow. The house features an exhaust air heat pump and under floor heating.

The house thermal characteristics were tested and a calibrated building simulation model developed, this was used to identify the parameters for a load shift equation. This equation estimated the day-ahead heating charge required to maintain comfort conditions (18–21 °C) based on the next day's forecast average temperature and solar radiation levels. This was implemented in a load shift controller system that operated the heat pump in the real test house.

The algorithm was initially tested using simulation, indicating that load shifting would not have a serious impact on thermal comfort, with conditions maintained between 18 and 21 °C for 84% of the time for the period 07:00–22:00 h.

The load shifting system was then implemented and tested in the house during September 2015 with results from the tests indicating that load shifting of the full space heating charge to off-peak-periods (00:00–07:00) was feasible for the test house without any substantial impact on thermal comfort during nominal occupied periods, with temperatures generally remaining between 19 °C and 23 °C. Peak temperatures were below 25 °C. However, significant solar gains occasionally pushed the upper floor temperature above 23 °C; as the heating charge had already been delivered to the floor slab, the system was unable to respond to this disturbance. Performance during the measured period was actually better than that suggested by simulation, with temperatures between 18 and 23 °C (0700–2200) for 87% of the time.

As the building was unoccupied during the tests, the impact of occupation was not accounted for – this would include heat gains from occupants and disturbances due to opening and closing external doors and windows. However, the same combination of modelling and testing could be used to develop new controller parameters and verify the efficacy of control in an occupied dwelling.

Despite comfortable conditions being maintained during load shifting, the measured energy performance of the house's exhaust air heat pump proved to be extremely poor. Analysis of the current drawn by the unit showed that the demand during off peak heating periods was approximately 5 kW; this indicated that almost all of the heat was supplied to the house was by the unit's auxiliary immersion heater (COP 1.0) rather than the heat pump itself, which has a nominal COP of 3. Subsequent investigation revealed that the compressor rarely switched on due to a low return water temperature alarm; something that is unavoidable with intermittent off-peak operation. It is unclear whether this problem is intrinsic to the design of the heat pump, or whether the control settings of the unit were poorly set during commissioning.

An enhanced load shift equation and calibration approach were developed to improve the day ahead energy predictions based on data collected from the monitoring equipment deployed in the test house.

Finally, a method for determining the amount of flexibility available on load-shifting was demonstrated using simulation, indicating that the ability to move a heating charge within a defined off-peak heating window diminished with increasing heating load for a fixed capacity heating system.

5. Limitations and future work

There are a number of areas where the work reported here could be further refined.

Subsequent field trials could analyse the operation of the enhanced load-shift controller and the flexible load-shifting algorithm in the test house to quantify any advantage over the original load-shift controller used in the field trials in this work.

The house was unoccupied during the controller test, so the impact of heat gains from occupants and occupant activity on the performance of the load-shifting algorithm could not be assessed; further research would require tests on an occupied house or at least include simulated occupancy.

The heating system tested here included under floor heating, which supports extensive time shifting of the thermal load. However, such underfloor heating is really only an option for load shifting in new housing. Experiments with the heat pump buffered using a storage tank would provide valuable insight into the performance and limits of load shifting when retrofitted into older house types.

The heat pump system control was limited to on and off switching. Future heat pump systems will feature compressors that can be modulated; allowing more nuanced manipulation of heat pump output to be implemented.

The exhaust air heat pump used in these trials was unable to operate effectively with intermittent operation. A more conventional air source heat pump system using outside air would be recommended for future trials.

Finally, the work reported here focused on space heating. In an occupied house the need for hot water heating would also need to be accommodated by the load shift controller.

Acknowledgements

This work was funded under the UK Grand Challenge Research Programme – Top and Tail of Energy Networks. The authors gratefully acknowledge the funding received from the Engineering and Physical Sciences Research Council (EPSRC) [grant number EP/I031707/1] and for the help given to them by other members of the consortium. The work also utilised technology developed under EPSRC grant EP/L024489/1.

The authors would like to acknowledge the generous help that they received from BRE Ltd. and Applegreen Homes Ltd. in making the test house available for the experiments reported in this paper.

The authors are also grateful for access to monitored climate data provided by Dr Paul Baker of Glasgow Caledonian University.

References

[1] Wilson IG, Rennie AJ, Ding Y, Eames PC, Hall PJ, Kelly NJ. Historical daily gas and electrical energy flows through Great Britain's transmission networks and the decarbonisation of domestic heat. Energy Policy 2013;61:301–5. http://dx.doi.org/10.1016/j.enpol.2013.05.110. ISSN 03014215.

[2] Callaway DS. Tapping the energy storage potential in electric loads to deliver load following and regulation, with application to wind energy. Energy Convers Manage 2009;50(5):1389–400. http://dx.doi.org/10.1016/j.enconman.2008.12.012. ISSN 01968904.

[3] Parkinson S, Wang D, Crawford C, Djilali N. Comfort-constrained distributed heat pump management. Energy Procedia 2011;12:849–55. http://dx.doi.org/10.1016/j.egypro.2011.10.112. ISSN 18766102.

[4] Wang D, Parkinson S, Miao W, Jia H, Crawford C, Djilali N. Online voltage security assessment considering comfort-constrained demand response control of distributed heat pump systems. Appl Energy 2012;96:104–14. http://dx.doi.org/10.1016/j.apenergy.2011.12.005. ISSN 03062619.

[5] Patteeuw D, Henze GP, Helsen L. Comparison of load shifting incentives for low-energy buildings with heat pumps to attain grid flexibility benefits. Appl Energy 2016;167(1):80–92.

[6] Hong J, Kelly NJ, Richardson I, Thomson M. The influence of thermal storage on microgeneration flexibility. In: 2nd international conference on microgeneration and associated technologies, Glasgow, UK.

[7] Hong J, Kelly NJ, Richardson I, Thomson M. Assessing heat pumps as flexible load. Proc Inst Mech Eng Part A: J Power Energy 2013;227(1):30–42. http://dx.doi.org/10.1177/0957650912454830.

[8] Arteconi A, Hewitt N, Polonara F. Domestic demand-side management (DSM): role of heat pumps and thermal energy storage (TES) systems. Appl Therm Eng 2013;51(1):155–65. http://dx.doi.org/10.1016/j.applthermaleng.2012.09.023. ISSN 13594311.

[9] Kelly NJ, Tuohy PG, Hawkes AD. Performance assessment of tariff based air source heat pump load shifting in a UK detached dwelling featuring phase change-enhanced buffering. Appl Therm Eng 2014;71(2):809–20. http://dx.doi.org/10.1016/j.applthermaleng.2013.12.019. ISSN 13594311.

[10] Renaldi R, Kiprakis A, Friedrich D. An optimisation framework for thermal energy storage integration in a residential heat pump heating system. Appl Energy 2017;186:520–9.

[11] Norford LK, Socolow RH, Hseih ES, Spadaro GV. Two-to-one discrepancy between measured and predicted performance of a 'low-energy' office building: insights from a reconciliation based on the DOE-2 model. Energy Build 1994;21(2):121–31.

[12] Knight I, Stravoravdis S, Lasvaux S. Assessing the operational energy profiles of UK education buildings: findings from detailed surveys and modelling compared to measured consumption. In: 2nd PALENC conference and 28th AIVC conference on building low energy cooling and advanced ventilation technologies in the 21st century, Crete Island, Greece. p. 531–6.

[13] Ryan Emily M, Sanquist Thomas F. Validation of building energy modeling tools under idealized and realistic conditions. Energy Build 2012;47:375–82.

[14] Clarke JA. Energy simulation in building design. 2nd ed. Oxford: Butterworth-Heinemann; 2001. ISBN 0750650826.

[15] Strachan P, Kokogiannakis G, Macdonald I. History and development of validation with the ESP-r simulation program. Build Environ 2008;43(4):601–9.

[16] Hensen JLM. On the thermal interaction of building structure and heating and ventilating systems [PhD Thesis]. Eindhoven University of Technology; 1991.

[17] Clarke JA, Kelly NJ. Integrating power flow modelling with building simulation. Energy Build 2001;V33(4):333–40.

[18] Araujo G, Sánchez E, Martí M. Determination of the two-exponential solar cell equation parameters from empirical data. Sol Cells 1982;5(2):199–204. http://dx.doi.org/10.1016/0379-6787(82)90027-8. ISSN 03796787.

[19] Rasmussen CE, Williams CKI. Gaussian processes for machine learning. Cambridge, Massachusetts: MIT Press; 2006. ISBN 026218253X <http://www.gaussianprocess.org/gpml/>.

[20] Zhang C, Wei H, Zhao X, Liu T, Zhang K. A Gaussian process regression based hybrid approach for short-term wind speed prediction. Energy Convers Manage 2016;126:1084–92. http://dx.doi.org/10.1016/j.enconman.2016.08.086. ISSN 01968904.

[21] Kou P, Liang D, Gao L, Lou J. Probabilistic electricity price forecasting with variational heteroscedastic Gaussian process and active learning. Energy Convers Manage 2015;89:298–308. http://dx.doi.org/10.1016/j.enconman.2014.10.003. ISSN 01968904.

[22] Monari F. Sensitivity analysis and Bayesian calibration of building energy models [Phd]. University of Strathclyde; 2016.

[23] Strbac G. Demand side management: benefits and challenges. Eng Policy 2008;36:4419–26.

[24] Lu N, Chassin DP. A state-queueing model of thermostatically controlled appliances. IEEE Trans Power Syst 2004;19(3):1666–73.

[25] Moreau A. Control strategy for domestic water heaters during peak periods and its impact on the demand for electricity. Energy Procedia 2011;12:1074–82.